


Microscopic study of the hot-fusion reaction $^{48}\text{Ca} + ^{238}\text{U}$ with the constraints from time-dependent Hartree-Fock theory

Xiang-Xiang Sun (孙向向)  and Lu Guo (郭璐)*

*School of Nuclear Science and Technology, University of Chinese Academy of Sciences, Beijing 100049, China
and CAS Key Laboratory of Theoretical Physics, Institute of Theoretical Physics, Chinese Academy of Sciences, Beijing 100190, China*

 (Received 13 February 2023; accepted 15 May 2023; published 22 June 2023)

Based on the microscopic descriptions of the ground state with static Hartree-Fock calculations and reaction dynamic using time-dependent Hartree-Fock (TDHF) theory, in combination with coupled-channel and fusion-by-diffusion models the capture and fusion processes of the hot-fusion reaction $^{48}\text{Ca} + ^{238}\text{U}$ are investigated. Considering the survival of the compound nucleus with statistical models, our calculations reproduce the experimental evaporation-residue cross sections. The orientation effects of ^{238}U are self-consistently included in the capture and fusion processes. With the internuclear potentials from the density-constrained frozen HF methods, the calculated capture cross sections agree well with the experimental data. The TDHF evolutions with different orientations and incident energies are used to extract the injection distance, which is the only input of the fusion-by-diffusion model for fusion probabilities. The fusion probabilities are strongly dependent on the orientations and the present calculations without any free parameters show that the tip-orientation collision is favorable for both the capture process and the formation of compound nucleus.

DOI: [10.1103/PhysRevC.107.064609](https://doi.org/10.1103/PhysRevC.107.064609)

I. INTRODUCTION

Extending the boundary of the nuclear chart is one of the most important and challenging topics in nuclear physics nowadays [1–4]. Up to now, in the laboratories the heaviest nuclei have been produced up to $Z = 118$ by using fusion-evaporation reactions: the cold-fusion reactions with ^{208}Pb and ^{209}Bi as targets for the synthesis of new elements up to $Z = 113$ [1,5] and hot-fusion reactions between ^{48}Ca and actinide nuclei for superheavy nuclei (SHN) with $113 \leq Z \leq 118$ [6,7], where Z is the proton number. Although many experimental efforts have been made to produce heavier SHN, however the synthesis of SHN with $Z \geq 119$ is still not achieved due to the extremely small cross sections and the limitation of experimental conditions [8–12].

A deep understanding of the fusion mechanism and a reliable prediction of cross sections are helpful to choose optimal combinations of projectile and target nuclei to produce new SHN. Conceptually, the fusion-evaporation reaction can be divided into three phases: the projectile overcomes the capture barrier leading to a dinuclear system, the touching configuration evolves to the compound nucleus (CN) by overcoming the inner barrier, and the excited CN survives against fission and the emission of light particle. For the capture process of cold- or hot-fusions, a dinuclear system can be directly formed in above-barrier reactions by overcoming the Coulomb barrier. Sub-barrier fusion can be regarded as a one-dimensional quantum tunneling under the internuclear potentials in the center of mass frame. The capture stage can be well

understood by using the empirical models or coupled-channels calculations [13–18]. For the formation of CN, the probabilities are very hard to be precisely determined experimentally [19] such that the experimental constraints on this process are deficient. The predictions from various methods, such as diffusion model [13], dinuclear system [20,21], and empirical formulas [16] differ by several orders of magnitude. Therefore a reliable prediction of fusion probabilities is significant to understand the mechanism of fusion-evaporation reactions. For the third process, the de-excitation of CN, the statistical models are commonly used to study the dependence of the survival probabilities on reaction parameters and it has been shown that the survival of CN is extremely sensitive to the height of fission barrier [16,22]. For the first and third processes, the relationship between incident-channel parameters and output have been well known and most of theoretical approaches have similar conclusions on them [13,16,20,21,23–32].

As for the formation of CN, the hindrance comes from the quasifission process where the touching configuration separates with a huge probability. Due to the difficulties in distinguishing the quasifission products of the dinuclear system and fission fragments of CN experimentally, it is extremely hard to extract the fusion probabilities from measurements such that the mechanism of the formation of CN is still not confirmed. The formation of the CN can be regarded as that the touching configuration overcomes the inner barrier to reach the saddle configuration. In the fusion-by-diffusion (FbD) model [13], this process is described as a thermal diffusion of a one-dimensional parabolic barrier from the injection point to the saddle point. Thus the fusion probabilities can be calculated with only one input parameter, the injection

*luguo@ucas.ac.cn

distance, which is determined by fitting to the experimental data [13,27,33,34]. This model has been successfully applied to cold- and hot-fusions [27,33,34] and orientation effects of the deformed target have also been considered [30]. But for the reactions without available experimental data, the predictive power might be influenced due to the adjustable parameter and the lack of dynamic information.

In fact, one can use modern dynamical microscopic approaches, such as the time-dependent Hartree-Fock (TDHF) theory, which can provide insight into the low-energy heavy-ion reactions (see Refs. [35–40] and references therein), including fusion and quasifission processes in reactions for the synthesis of SHN [41–52], to restrict the inputs for the description of fusion evaporation reactions. It has been shown that the TDHF simulations can provide the main ingredients of coupled-channels calculations for capture cross section [40,53–57] and diffusion processes [58]. The advantages of such strategy are that one can eliminate the uncertainties caused by adjustable parameters for calculating capture and fusion cross sections under the restriction from microscopic TDHF theory, meanwhile the influences of the structures of reactants and dynamical effects can be taken into account. Thus it is feasible to study the systematics of evaporation-residue cross sections based on microscopic descriptions of reaction dynamics.

In our previous work [59], we have combined the TDHF theory with FbD model to describe the systematics of fusion cross sections of three cold-fusion reactions. We extract the only input of the FbD model, the energy-dependent injection distance by using TDHF simulation and our calculations can well describe the fusion probabilities restricted by the experimental data from Ref. [60]. As for the capture process, the internuclear potentials with the form of Woods-Saxon type are also restricted by microscopic information. In the present work, we extend and improve the method shown in Ref. [59] to study the evaporation-residue cross sections of hot-fusion reactions. We calculate the internuclear potentials by using the density-constrained frozen HF method [56] and then use them to get the capture cross sections with the orientation-average formula. For hot-fusion reactions, to study the orientation effects of deformed target on the fusion process, we carry out the TDHF calculations with different orientations and incident energies to extract the injection distances, which are used to get fusion probabilities using the FbD model. We include the de-excitation of CN by statistical model. The hot-fusion reaction $^{48}\text{Ca} + ^{238}\text{U}$ is investigated to check the effectiveness of our model.

This article is organized as follows. In Sec. II, we show the main theoretical formulation to calculate capture cross sections, fusion probabilities, and survival probabilities. Section III presents the calculational details, the discussion of orientation effects on capture and fusion processes, and evaporation-residue cross sections of $^{48}\text{Ca} + ^{238}\text{U}$. We summarize our work and give a brief perspective in Sec. IV.

II. THEORETICAL FRAMEWORK

We start from the TDHF theory, in which the Hamiltonian \hat{H} is a functional of various densities and the dynamic process

is described by the evolution of the nucleon density $\hat{\rho}$ with the TDHF equation

$$i\hbar \frac{\partial}{\partial t} \hat{\rho} = [\hat{H}[\hat{\rho}], \hat{\rho}]. \quad (1)$$

Since the TDHF theory describes the collective motion in a semiclassical way, the quantum tunneling of the many-body wave function is not included. Therefore when studying capture cross sections by using the TDHF theory, a commonly applied and very effective approach is using the internuclear potential obtained from frozen density approximation [61], density constrained (DC) TDHF [53,62–64], and DC frozen HF [56], as the input of the coupled-channels code CCFULL [65] to calculate the penetration probability.

In our previous work [59] for cold-fusion reactions, the internuclear potentials are the form of the Woods-Saxon type with involving parameters determined by fitting to the matter radii and capture threshold from TDHF calculations. In the present work, we directly use the DC-FHF method to calculate the internuclear potentials for hot-fusion reactions without any adjustable parameters. Most of the reactants of hot-fusion reactions are deformed such that the orientation effects should be considered. In the DC-FHF method, the HF calculations are performed with constraining the total proton p and neutron n densities to be the same as those of the ground state,

$$\delta \left\langle H - \int d^3r \sum_{q=p,n} \lambda_q(\mathbf{r}) [\rho_{p,q}(\mathbf{r}; \theta_p) + \rho_{T,q}(\mathbf{r} - \mathbf{R}; \theta_T)] \right\rangle = 0, \quad (2)$$

where $\rho_p(\theta_p)$ and $\rho_T(\theta_T)$ are densities of the projectile and target for a given orientation labeled by (θ_p, θ_T) , which can be achieved by performing Eulerian rotations of Slater determinants in a three-dimensional Cartesian geometry [66]. θ_p (θ_T) denotes the angle between the symmetry axis of the deformed projectile (target) and the collision axis in head-on reaction. \mathbf{R} is the vector between two centers of mass of projectile and target. This variation procedure results in a unique Slater determinant $\Phi(\mathbf{R})$. The internuclear potential is given by

$$V_{\text{DC-FHF}}(\mathbf{R}; \theta_p, \theta_T) = \langle \Phi(\mathbf{R}) | H | \Phi(\mathbf{R}) \rangle (\theta_p, \theta_T) - E_p - E_T, \quad (3)$$

where E_p and E_T are the binding energies of projectile and target, respectively. Subsequently, the penetration probabilities $T_J(E_{\text{c.m.}})$, corresponding to orbital angular momentum J , are obtained by solving the Schrödinger equation

$$\left[\frac{-\hbar^2}{2\mu} \frac{d^2}{dR^2} + \frac{J(J+1)\hbar^2}{2\mu R^2} + V_{\text{DC-FHF}}(R) - E_{\text{c.m.}} \right] \psi(R) = 0 \quad (4)$$

with the incoming wave boundary condition method [65]. The capture cross sections at below- and above-barrier regions for each orientation (θ_T, θ_p) are then calculated as

$$\sigma_{\text{cap}}(E_{\text{c.m.}}, \theta_T, \theta_p) = \frac{\pi}{k^2} \sum_J (2J+1) T_J(E_{\text{c.m.}}), \quad (5)$$

where $k = \sqrt{2\mu E_{c.m.}/\hbar^2}$ with μ being the reduced mass in the entrance channel.

The orientation-average cross section is given as

$$\sigma_{\text{cap}}(E_{c.m.}) = \int_0^1 d \cos(\theta_P) \int_0^1 d \cos(\theta_T) \times \frac{\pi}{k^2} \sum_J (2J+1) T_J(E_{c.m.}, \theta_P, \theta_T). \quad (6)$$

It should be noted that this formula is valid for systems in which both projectile and target nuclei are axially deformed without reflection asymmetric shapes, meanwhile the collision direction and the principle axes of the target and projectile are in the same plane.

For the second stage of the fusion-evaporation reactions, the contact configuration of touching nuclei can be transformed to CN configuration by overcoming the inner barrier. In this process, before the formation of CN, quafission happens and the heavy nuclear system splits into two fragments. Therefore, the formation of CN is strongly hindered by quafission. In our previous work [59] the fusion-by-diffusion (FbD) model [13,27,33,67] is used to calculate the fusion probabilities $P_{\text{CN}}(E_{c.m.}, J)$ of cold-fusion reactions, which are totally determined by the distance between the surfaces of two colliding nuclei at the injection point. We have shown that the calculated fusion probabilities are consistent with the measurements for cold-fusion reactions [59]. The injection distance can be estimated from the TDHF evolution by choosing the moment when the collective kinetic energy is completely dissipated into the internal degrees of freedom in the overdamped regime for a given incident energy. For hot-fusion reactions, the reactants are deformed therefore the orientation effects on fusion probabilities should be considered, which have been formulated in Ref. [30] within the framework of FbD. In this work, we combine the formulas given in Ref. [30] with the TDHF evolution to determine the fusion probability of hot-fusion systems. In the FbD model, the formation of compound nuclei is described as a diffusion process under an inverted parabolic potential barrier

$$V_J(s) = V_{\text{fiss}}(s) + \frac{J(J+1)}{2\mathcal{I}(s)}, \quad (7)$$

where s is the surface separation distance between the two colliding nuclei, $V_{\text{fiss}}(s)$ is the inner fission potential, and $\mathcal{I}(s)$ is the moment of inertia for the mononuclear system. For a given orientation, the fusion probability is calculated as

$$P_{\text{CN}}(\theta_P, \theta_T, E_{c.m.}, J) = \frac{1}{2} \left[1 - \text{erf} \left(\frac{\Delta V_J(\theta_P, \theta_T)}{T_J(\theta_P, \theta_T)} \right) \right], \quad (8)$$

where $\Delta V_J(\theta_P, \theta_T)$ is the effective barrier height for the fusion process

$$\Delta V_J(\theta_P, \theta_T) = V_J(s_{\text{sad}}) - V_J[s_{\text{inj}}(\theta_P, \theta_T)], \quad (9)$$

and T is the temperature

$$T_J(\theta_P, \theta_T) = \sqrt{T_J(J, s_{\text{sad}}) T_J[s_{\text{inj}}(\theta_P, \theta_T)]}. \quad (10)$$

s_{sad} is the surface separation distance at the saddle point and s_{inj} for the injection point, which is dependent on the orientations [30] for deformed systems. For a given s and J , the

temperature can be calculated as

$$T_J(s) = \sqrt{\frac{E_{\text{CN}}^* - V_J(s) - E_{\text{pair}}}{a(s)}}, \quad (11)$$

where $a(s)$ is the level density parameter and E_{pair} for pairing energy, which is taken to be $21/\sqrt{A}$ for even-even nuclei, $10.5/\sqrt{A}$ for odd-mass nuclei, and 0 for odd-odd nuclei with the mass number A . The excitation energy of the compound nuclei is $E_{\text{CN}}^* = E_{c.m.} - M_{\text{CN}}c^2 + M_Pc^2 + M_Tc^2$. See Refs. [13,27,67] for the parametrization of the inner barrier, the moment of inertia, temperature used in the FbD model, and level density parameter.

After getting the fusion probability, we can calculate fusion cross section by

$$\sigma_{\text{fus}}(E_{c.m.}) = \int_0^1 d \cos(\theta_P) \int_0^1 d \cos(\theta_T) \times \frac{\pi}{k^2} \sum_J (2J+1) T_J(E_{c.m.}, \theta_P, \theta_T) \times P_{\text{CN}}(\theta_P, \theta_T, E_{c.m.}, J). \quad (12)$$

Thus, one can study the systematics of the fusion probability by comparing the effective fusion probabilities P_{fus} calculated by

$$P_{\text{fus}}(E_{c.m.}) = \frac{\sigma_{\text{fus}}(E_{c.m.})}{\sigma_{\text{cap}}(E_{c.m.})} \quad (13)$$

with measured ones.

For the survival probability of the compound nuclei, here, we only consider the competition of neutron emission and fission. The survival probability of emitting x neutrons can be written as

$$W_{\text{sur}}(E_{\text{CN}}^*, x, J) = P(E_{\text{CN}}^*, x) \prod_i^x \left(\frac{\Gamma_n(E_i^*, J)}{\Gamma_n(E_i^*, J) + \Gamma_f(E_i^*, J)} \right), \quad (14)$$

where $\Gamma_n(E_i^*, J)$ and $\Gamma_f(E_i^*, J)$ are the neutron-evaporation and fission width at an excitation energy E_i^* and angular momentum J , which are calculated with the formulas in Refs. [68,69]. E_i^* is the excitation energy before evaporating the i th neutron. The realization probability $P(E_{\text{CN}}^*, x)$ is given by the formula of neutron evaporation proposed by Jackson [70] when $x > 1$. The realization probability of the case of 1n channel reads [23]

$$P(E_{\text{CN}}^*, 1) = \exp[-(E_{\text{CN}}^* - B_n - 2T)^2/2\Sigma^2], \quad (15)$$

where $T = [1 + \sqrt{1 + 4aE_{\text{CN}}^*}]/2a$ is the temperature of the nucleus, the width of excitation function $\Sigma = 2.5$ MeV, and B_n denotes the binding energy of the emitted neutron with the residue nucleus. The neutron-evaporation and fission width are dependent on level density, which is calculated with the Fermi-gas model. More details of this part can be found in Ref. [23].

Thus in this paper, the evaporation residue cross section for x neutrons (xn) channel is

$$\begin{aligned} \sigma_{\text{ER}}(E_{\text{c.m.}}, x) &= \int_0^1 d \cos(\theta_P) \int_0^1 d \cos(\theta_T) \\ &\times \frac{\pi}{k^2} \sum_J (2J+1) T_J(E_{\text{c.m.}}, \theta_T, \theta_P) \\ &\times P_{\text{CN}}(\theta_P, \theta_T, E_{\text{c.m.}}, J) W_{\text{sur}}(E_{\text{CN}}^*, x, J). \end{aligned} \quad (16)$$

III. RESULTS AND DISCUSSIONS

As mentioned above, we calculate the capture cross sections with the orientation-average formula after getting the penetration probabilities under the internuclear potential from the DC-FHF method. We have implemented the DC-FHF method [56] based on our modified version of the Sky3D code [71], which recently has been used to study the fusion reactions [40,59,72], multinucleon transfer reactions [73–75], quasifission [52], and the effects of tensor force on reactions mechanism [57,62–64,76]. In the DC-FHF method, we calculate the ground state wave functions of projectile and target by solving the static HF equation on a three-dimensional grid $28 \times 28 \times 28 \text{ fm}^3$ with the spacing of 1 fm in each direction. The density functional SLy5 [77] is adopted in both static and dynamic calculations. The ground state of ^{48}Ca has a spherical shape and the root-mean-square matter radius is 3.56 fm. The ground state of ^{238}U is prolate with the quadrupole deformation, β_2 , the hexadecapole deformation β_4 , and the hexacontatetrapole deformation β_6 of 0.291, 0.185, and 0.063, respectively, and the root-mean-square matter radius is 5.92 fm. The ground state density distributions of ^{48}Ca and ^{238}U can be seen in Fig. 4(a). Since the ground state of ^{48}Ca has a spherical shape, the potentials only depend on the orientations of ^{238}U , labeled as θ in the following. By putting the ground state wave functions into a bigger three-dimensional grid of $56 \times 40 \times 40 \text{ fm}^3$ and using the DC-FHF method, Fig. 1 shows the internuclear potentials for selected orientations of ^{238}U . In the DC-FHF calculations, the distance between centers of mass of projectile and target ranges from

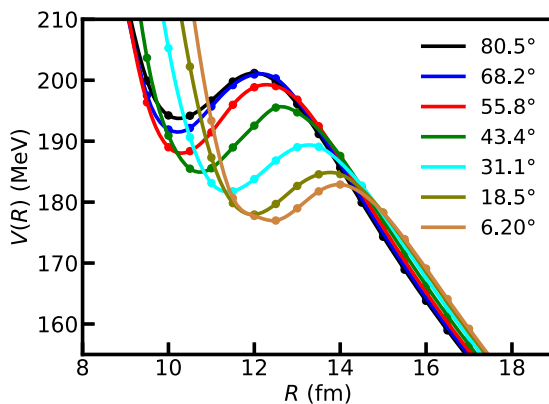


FIG. 1. Internuclear potentials between ^{48}Ca and ^{238}U for different orientations labeled by the orientation angle of ^{238}U by using the DC-FHF method.

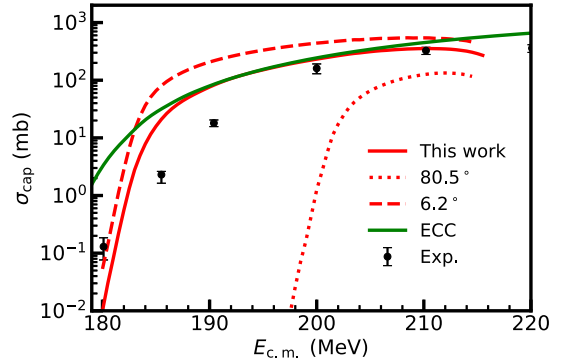


FIG. 2. Capture cross sections σ_{cap} of $^{48}\text{Ca} + ^{238}\text{U}$ as a function of incident energies. The experimental data (solid circles) are taken from Ref. [79]. The calculations with the empirical coupled-channel (ECC) model [17] are shown by the green line. Our calculations using Eq. (6) are shown by the red solid line and the cross sections for $\theta = 83.8^\circ$ and $\theta = 9.5^\circ$ are presented by dash-dotted and dashed lines.

25 fm to 5 fm with the step size of 0.5 fm. The integral in Eq. (6) is calculated by seven points Gaussian quadrature in the range of $[0, \pi/2]$. Thus we present seven potentials labeled by orientation angles in Fig. 1. It is clear that the potentials from DC-FHF naturally include the repulsive core due to the Pauli principle being considered in the variation procedures compared with the case of frozen density approximation. Usually the capture barrier height of side orientation is obviously larger than that of tip orientation, which can be clearly drawn in our calculations. Additionally, the internuclear potentials from DC-FHF only depend on the adopted nucleon-nucleon effective interaction and do not contain any free parameters. We would like to mention that the potentials from DC-FHF is very close to the potentials from empirical formulas such as the results given in Ref. [78], which implies that the description of capture cross sections of our method will be similar to the empirical models.

In Fig. 2, we show the calculated cross sections and the comparison with the results from the empirical coupled-channel (ECC) model [17] and experimental data taken from Ref. [79]. Generally speaking, our calculations can well reproduce the measurements and our results for incident energies smaller than 190 MeV are better than those of ECC. This means that our no-free parameter calculations starting from effective nucleon-nucleon interaction can well describe the capture process, even better than the empirical model with several adjusted parameters. In Fig. 2, we also present the capture cross sections with the orientation angles of ^{238}U of 9.3° and 83.8° . The former is close to the tip collision and the latter is close to side collision. It is clear that captures cross section of tip orientation is much larger than those of side collision due to the lower capture barrier.

To calculate the fusion probabilities by using the FbD model, as we mentioned, one needs to extract the injection distance from the TDHF simulation. For the dynamic evolution of the reaction $^{48}\text{Ca} + ^{238}\text{U}$, we carry out the calculations on the three-dimensional grid of $56 \times 40 \times 40 \text{ fm}^3$ and the time spacing is 0.2 fm/c. The incident energies are in the

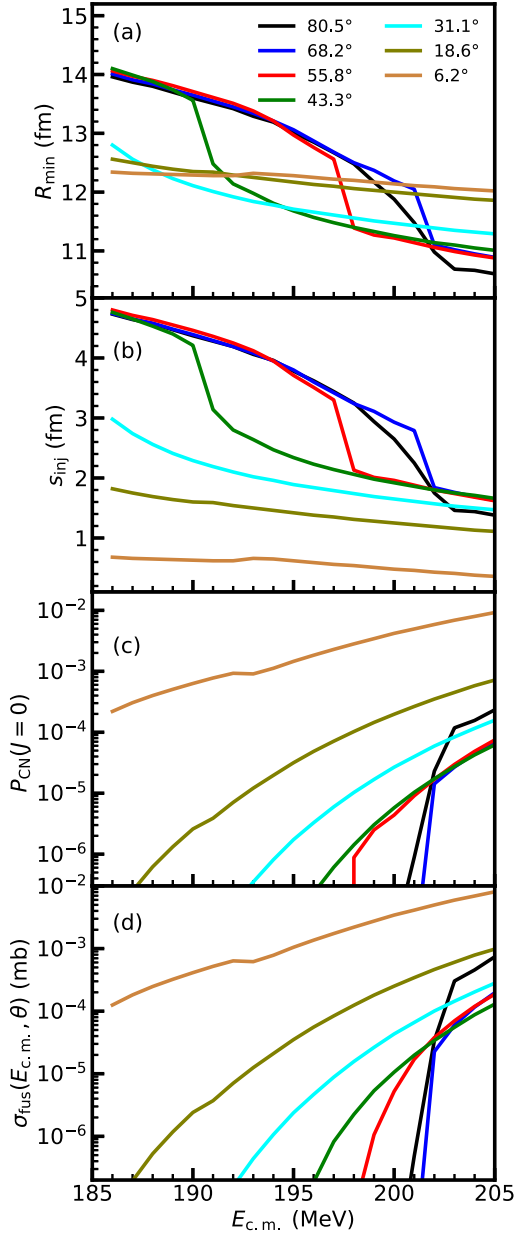


FIG. 3. Separation distance of centers of mass of two fragments with zero conjugate momenta (a), injection distances (b), fusion probabilities with zero angular momentum (c), and fusion cross sections (d) for different orientations as a function of incident energies for the $^{48}\text{Ca} + ^{238}\text{U}$ reaction.

range [186,205] MeV with the step of 1 MeV. This means that we have totally calculated 140 dynamic processes after considering the orientations of the deformed target ^{238}U . For each TDHF simulation with the fixed incident energy and orientation angle, following the method given in Ref. [59], we can get the separation distance R_{\min} defined as the distance between centers of mass of two fragments at the injection configuration which corresponds to the moment with zero conjugate momentum. The calculated results are shown in Fig. 3(a) for each orientation. We find that there is a sudden decrease of R_{\min} when $E_{c.m.}$ is close to the capture barrier

for a fixed orientation. For the orientations close to the side collision with the capture barriers about 200 MeV, when the incident energies are smaller than capture barrier, the values of R_{\min} are close to each other. For those orientations close to tip case, the capture barriers are about 185 MeV, we find that R_{\min} decreases slowly with $E_{c.m.}$. When the incident energies are larger than the capture barrier of side orientation, e.g., $E_{c.m.} = 205$ MeV, R_{\min} increases with the orientation angles. For a given orientation, R_{\min} decreases with $E_{c.m.}$ more slowly in the above-barrier region than in the sub-barrier region and has a jump near the Coulomb barrier, which is similar to conclusions given in Ref. [59] for cold fusions.

After obtaining R_{\min} , we can get the injection distances s_{inj} . The nuclear surface can be well described by using the spherical harmonic expansions and for the axially deformed nuclei, in the reaction plane one has

$$R_T(\theta) = R_T [1 + \beta_2 Y_{20}(\theta) + \beta_4 Y_{40}(\theta) + \beta_6 Y_{60}(\theta)]. \quad (17)$$

Thus we can calculate the injection distance by

$$s_{\text{inj}}(\theta, E_{c.m.}) = R_{\min}(\theta, E_{c.m.}) - R_P - R_T(\theta). \quad (18)$$

R_P and R_T are the mass radius from static HF calculations. We would like to mention that such treatment is similar to those in Ref. [30]. The obtained results of s_{inj} are presented in Fig. 3(b). The overall tendency for each orientation is similar to that of R_{\min} . The injection distance for the orientations close to tip one is smaller than those close to side orientation, which is contrary to the results shown in Ref. [30], where the injection distance without considering the orientation is calculated by the empirical formulas and the injection distance with the orientation effects almost decreases with the orientation angles. In our calculations, the values of R_{\min} determined from TDHF simulations are strongly related to the orientations. Therefore the effects of reaction dynamics on R_{\min} is considered and the change of R_{\min} is also related to the height of capture barriers. For tip orientation, the lower limit of the incident energy in question is always larger than the capture barriers, therefore the system has enough energy to overcome the barrier and the contact configuration is reached. For those collisions close to side orientation, since the corresponding capture barriers belong to the interval [186, 205] MeV, in below-barrier energies elastic scattering happens such that the injection distances are obviously larger than those of tip orientation.

More interesting, by comparing two typical orientations in which the contact configurations are formed, the injection distance of orientations close to tip one is also smaller than those with orientations close to side case. To understand this, in Figs. 4 and 5 we show the density evolution of tip and side collisions with the same incident energy 205 MeV. The static shapes of the projectile and target are indicated by the solid red and black lines. Figures 4(a) and 5(a) show the initial configurations and Figs. 4(b) and 5(b) for a selected phase in the approaching process. In Figs. 4(c) and 5(c) we show the moment with about zero collective kinetic energy of the system, which is used to get the injection distance. Along the reaction direction (x axis), the distance from the center of mass of the target nucleus to the nuclear surface in the tip orientation is larger than that of side orientation by

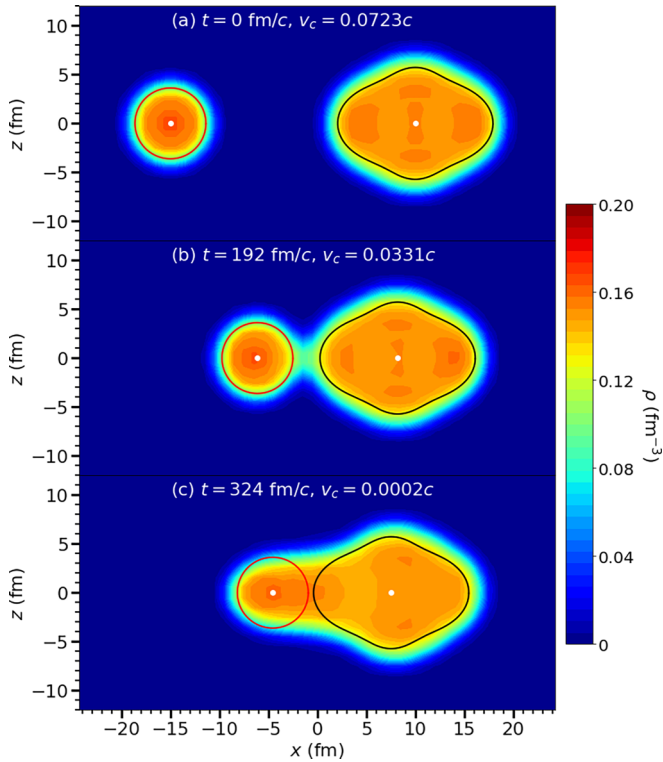


FIG. 4. Two-dimensional density distributions of $^{48}\text{Ca} + ^{238}\text{U}$ with ^{238}U being tip orientation at three selected moments during the TDHF evolution. The time t and corresponding speed v_c for the center of mass of the reaction system are given. The red and black lines represent the shapes of the projectile and target in the reaction plane (the xz plane). The white points label the centers of mass of two fragments. The incident energy is taken to be 205 MeV.

about 2 fm. But the difference of R_{\min} between tip and side orientation is about 1.2 fm. Therefore the injection distance of tip orientation is smaller than that of side orientation. We also find that the tip collision can more quickly approach the phase with zero collective kinetic energy than side collision, which can be understood as overcoming the capture barrier, the tip orientation still has enough push to reach the injection configuration in the one-dimension diffusion model. We would like to mention that in the present way to get the injection distance we assume a frozen shape of target and projectile, but in the dynamic evolution to form a compact configuration the system undergoes a complex change of shape and exchange of nucleons through the neck. The influence of these factors on injection distance is still very difficult to take into account. The advantage of our methods is that the results of injection parameter, which is the only input of the FbD model for fusion probability, are determined by microscopic TDHF theory without any adjustable parameters. From the view of point of the exchange of nucleons between target and projectile, the side collision has a longer contact time thus is favorable to the transfer of nucleons, which may also influence the fusion probabilities but its effects cannot be studied using a one-dimension diffusion model.

After getting the injection distances, the fusion probabilities can be determined by the FbD model and the smaller

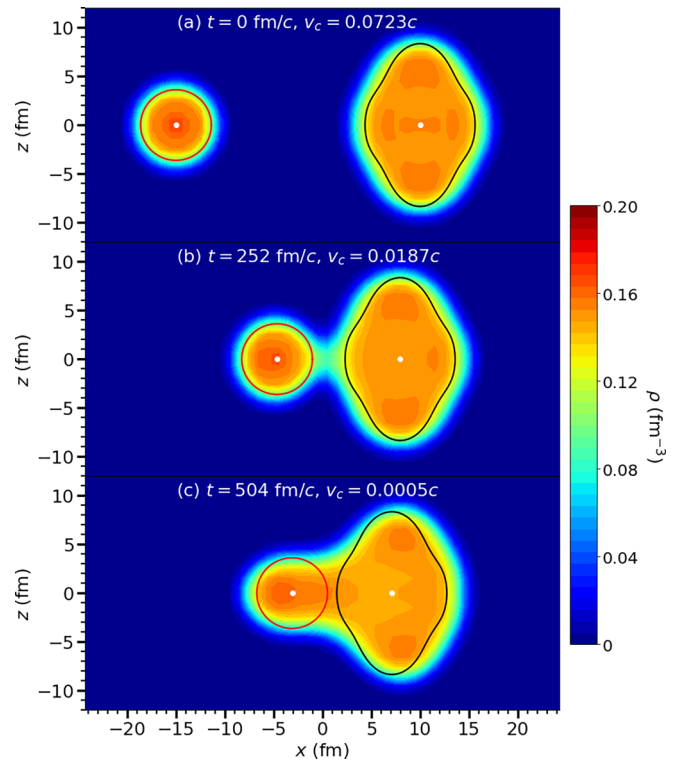


FIG. 5. Same to Fig. 4 but for the side orientation of ^{238}U .

injection distances correspond to larger probabilities of the formation of compound nucleus. In Fig. 3(c) we display the calculated fusion probabilities with zero angular momenta for different orientations. The formation probabilities with orientations close to tip case are larger than those with side orientations due to the smaller injection distances. We also find that the formation probabilities are also strongly dependent on the orientations, similar to the case of injection distances. From the tip orientation to the side one, the fusion probabilities decrease and then increase when the incident energy is close to 205 MeV. In Fig. 3(d) we present the fusion cross sections for each orientation and it is clearly that the tip orientation is more favorable for the formation of compound nucleus from our TDHF+FbD calculations. It should be mentioned that by only using TDHF simulation, it has been shown in Refs. [44,80,81] that the tip-orientation collisions cannot lead to the formation of CN while the side-orientation ones have longer contact time for same incident energies. But in these works, the systematics of fusion probabilities are not provided. Therefore it is necessary to consider more dynamic factors and to investigate how they influence the fusion probabilities toward a more realistic and deep understanding of the complex fusion mechanisms.

With considering the average of orientation angles, we can get the total fusion cross sections [cf. Eq. (12)] and effective fusion probabilities [cf. Eq. (13)] of the reaction $^{48}\text{Ca} + ^{238}\text{U}$, which are shown in Fig. 6. Our calculated effective fusion probabilities ($2\text{--}6 \times 10^{-4}$) are close to the calculations in Ref. [78] by using the dinuclear system model. The fusion cross sections increase slowly with incident energies. For the calculation of survival probabilities, we only consider the

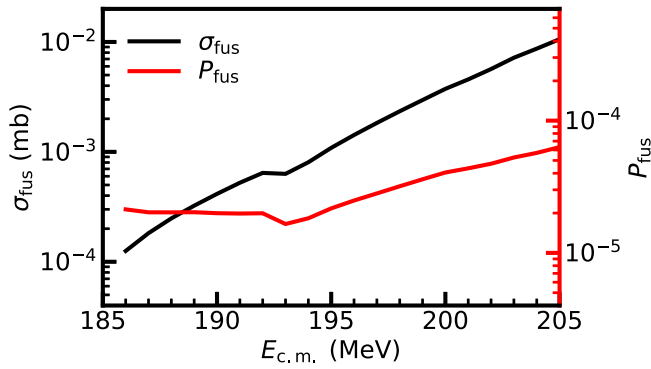


FIG. 6. Orientation-averaged fusion cross sections (black line) and effective fusion probabilities (red line) for the reaction $^{48}\text{Ca} + ^{238}\text{U}$ as a function of incident energies.

competition between fission and neutron emission and the fission barrier height. The inputs including neutron-separation energies are taken from the newest microscopic-macroscopic model results [82]. In Fig. 7, we show the evaporation-residue cross sections in $3n$ and $4n$ channels and the comparison with experimental data taken from Refs. [3,83]. It should be noted that the datum around 195 MeV is a “upper cross section limit” [83]. One can find that our calculations are generally in good agreement with the measurements of the reaction $^{48}\text{Ca} + ^{238}\text{U}$. This reflects that the combination of microscopic TDHF theory with the FbD model for fusion process and the statistical model for survival of compound nucleus is a valid approach to describe hot-fusion reactions.

IV. SUMMARY AND PERSPECTIVE

To summarize, we have studied the fusion-evaporation reaction $^{48}\text{Ca} + ^{238}\text{U}$ based on a microscopic description of the reaction dynamics using the TDHF theory. For the

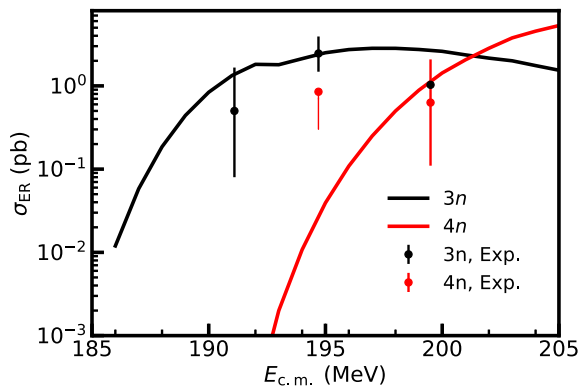


FIG. 7. Evaporation-residue cross sections as a function of the incident energy in the center-of-mass frame for the hot-fusion reaction $^{48}\text{Ca} + ^{238}\text{U}$. The $3n$ and $4n$ channels are labeled by black and red lines. The experimental data are taken from Refs. [3,83].

capture process, we calculate the internuclear potentials of $^{48}\text{Ca} + ^{238}\text{U}$ for different orientations of deformed target by using the DC-FHF method and the capture cross sections are treated by the orientation-average formula. The results of capture process show a nice agreement with the experimental data and are even better than the empirical models. For the formation probabilities of the compound nucleus, we use the FdD model with the only input parameter, the injection distance, which is determined from the TDHF simulation for head-on collisions with considering the orientation effects. Our calculations show that the tip orientation is more favorable to both capture process and the formation of the compound nucleus, leading to large fusion cross sections of tip collision. We would like to mention that there are no adjustable parameters in the description of the above two processes in our treatment. For the survival of the compound nucleus, we use the statistical model with the fission barrier and neutron separation energies from microscopic-macroscopic model. As a results, our calculations of $^{48}\text{Ca} + ^{238}\text{U}$ can reproduce the experimental evaporation-residue cross sections.

In our method, the injection parameters are determined by assuming that the surfaces of the target and projectile are frozen. Actually, the dynamic process of fusion reactions is very complicated and the formation of the compound nucleus from contact configuration undergoes complex evolution of shape degrees of freedom accompanied with the exchange of nucleons. Thus it would be more accurate if more dynamic factors can be considered when extracting this injection parameter. Furthermore, one can combine the TDHF with more complex diffusion models to treat the second phase of fusion reaction. Reasonably taking into account more dynamic effects can certainly improve our knowledge of heavy-ion fusion reactions for the synthesis of superheavy nuclei. This is our long goal and further works are necessary.

The present work is a natural extension of our previous investigation [59], in which the fusion probabilities of cold-fusion are studied by including the orientation effects and the survival process. Thus the method presented in this paper can be applied to other hot-fusion systems. In the coming work, we will apply this approach to choose the optimal combination of target and projectile nuclei for the synthesis of the SHN with $Z = 119$ and $Z = 120$.

ACKNOWLEDGMENTS

We thank Bing Wang and Shan-Gui Zhou for helpful discussions and suggestions. This work has been supported by the Strategic Priority Research Program of Chinese Academy of Sciences with Grant No. XDB34010000, the National Natural Science Foundation of China with Grants No. 11975237 and No. 12205308, and the Fundamental Research Funds for the Central Universities with Grant No. E2E46302. The computations in this paper have been performed on the High-performance Computing Cluster of Institute of Theoretical Physics, Chinese Academy of Sciences.

- [1] S. Hofmann and G. Münzenberg, *Rev. Mod. Phys.* **72**, 733 (2000).
- [2] J. H. Hamilton, S. Hofmann, and Y. T. Oganessian, *Annu. Rev. Nucl. Part. Sci.* **63**, 383 (2013).
- [3] Y. T. Oganessian and V. K. Utyonkov, *Rep. Prog. Phys.* **78**, 036301 (2015).
- [4] S. A. Giuliani, Z. Matheson, W. Nazarewicz, E. Olsen, P.-G. Reinhard, J. Sadhukhan, B. Schuettrumpf, N. Schunck, and P. Schwerdtfeger, *Rev. Mod. Phys.* **91**, 011001 (2019).
- [5] K. Morita, K. Morimoto, D. Kaji, T. Akiyama, S.-i. Goto, H. Haba, E. Ideguchi, R. Kanungo, K. Katori, H. Koura, H. Kudo, T. Ohnishi, A. Ozawa, T. Suda, K. Sueki, H.-S. Xu, T. Yamaguchi, A. Yoneda, A. Yoshida, and Y.-L. Zhao, *J. Phys. Soc. Jpn.* **73**, 2593 (2004).
- [6] Y. Oganessian, *J. Phys. G: Nucl. Part. Phys.* **34**, R165 (2007).
- [7] Y. T. Oganessian, F. S. Abdullin, P. D. Bailey, D. E. Benker, M. E. Bennett, S. N. Dmitriev, J. G. Ezold, J. H. Hamilton, R. A. Henderson, M. G. Itkis, Y. V. Lobanov, A. N. Mezentsev, K. J. Moody, S. L. Nelson, A. N. Polyakov, C. E. Porter, A. V. Ramayya, F. D. Riley, J. B. Roberto, M. A. Ryabinin *et al.*, *Phys. Rev. Lett.* **104**, 142502 (2010).
- [8] Y. T. Oganessian, V. K. Utyonkov, Y. V. Lobanov, F. S. Abdullin, A. N. Polyakov, R. N. Sagaidak, I. V. Shirokovsky, Y. S. Tsyganov, A. A. Voinov, A. N. Mezentsev, V. G. Subbotin, A. M. Sukhov, K. Subotic, V. I. Zagrebaev, S. N. Dmitriev, R. A. Henderson, K. J. Moody, J. M. Kenneally, J. H. Landrum, D. A. Shaughnessy *et al.*, *Phys. Rev. C* **79**, 024603 (2009).
- [9] E. M. Kozulin, G. N. Knyazheva, I. M. Itkis, M. G. Itkis, A. A. Bogachev, L. Krupa, T. A. Loktev, S. V. Smirnov, V. I. Zagrebaev, J. Äystö, W. H. Trzaska, V. A. Rubchenya, E. Vardaci, A. M. Stefanini, M. Cinausero, L. Corradi, E. Fioretto, P. Mason, G. F. Prete, R. Silvestri *et al.*, *Phys. Lett. B* **686**, 227 (2010).
- [10] S. Hofmann, S. Heinz, R. Mann, J. Maurer, G. Münzenberg, S. Antalic, W. Barth, H. G. Burkhard, L. Dahl, K. Eberhardt, R. Grzywacz, J. H. Hamilton, R. A. Henderson, J. M. Kenneally, B. Kindler, I. Kojouharov, R. Lang, B. Lommel, K. Miernik, D. Miller *et al.*, *Eur. Phys. J. A* **52**, 180 (2016).
- [11] J. Khuyagbaatar, A. Yakushev, Ch. E. Düllmann, D. Ackermann, L.-L. Andersson, M. Asai, M. Block, R. A. Boll, H. Brand, D. M. Cox, M. Dasgupta, X. Derkx, A. Di Nitto, K. Eberhardt, J. Even, M. Evers, C. Fahlander, U. Forsberg, J. M. Gates, N. Gharibyan *et al.*, *Phys. Rev. C* **102**, 064602 (2020).
- [12] H. M. Albers, J. Khuyagbaatar, D. J. Hinde, I. P. Carter, K. J. Cook, M. Dasgupta, Ch. E. Düllmann, K. Eberhardt, D. Y. Jeung, S. Kalkal, B. Kindler, N. R. Lobanov, B. Lommel, C. Mokry, E. Prasad, D. C. Rafferty, J. Runke, K. Sekizawa, C. Sengupta, C. Simenel *et al.*, *Phys. Lett. B* **808**, 135626 (2020).
- [13] W. J. Świątecki, K. Siwek-Wilczyńska, and J. Wilczyński, *Phys. Rev. C* **71**, 014602 (2005).
- [14] K. Hagino and N. Takigawa, *Prog. Theor. Phys.* **128**, 1061 (2012).
- [15] B. B. Back, H. Esbensen, C. L. Jiang, and K. E. Rehm, *Rev. Mod. Phys.* **86**, 317 (2014).
- [16] V. I. Zagrebaev and W. Greiner, *Nucl. Phys. A* **944**, 257 (2015).
- [17] B. Wang, K. Wen, W.-J. Zhao, E.-G. Zhao, and S.-G. Zhou, *At. Data Nucl. Data Tables* **114**, 281 (2017).
- [18] K. Hagino, K. Ogata, and A. M. Moro, *Prog. Part. Nucl. Phys.* **125**, 103951 (2022).
- [19] D. Hinde, M. Dasgupta, and E. Simpson, *Prog. Part. Nucl. Phys.* **118**, 103856 (2021).
- [20] N. V. Antonenko, E. A. Cherepanov, A. K. Nasirov, V. P. Permjakov, and V. V. Volkov, *Phys. Lett. B* **319**, 425 (1993).
- [21] G. G. Adamian, N. V. Antonenko, W. Scheid, and V. V. Volkov, *Nucl. Phys. A* **627**, 361 (1997).
- [22] G. G. Adamian, N. V. Antonenko, S. P. Ivanova, and W. Scheid, *Phys. Rev. C* **62**, 064303 (2000).
- [23] Z.-Q. Feng, G.-M. Jin, F. Fu, and J.-Q. Li, *Nucl. Phys. A* **771**, 50 (2006).
- [24] L. Zhu, W.-J. Xie, and F.-S. Zhang, *Phys. Rev. C* **89**, 024615 (2014).
- [25] N. Wang, E.-G. Zhao, W. Scheid, and S.-G. Zhou, *Phys. Rev. C* **85**, 041601(R) (2012).
- [26] Z.-H. Liu and J.-D. Bao, *Phys. Rev. C* **84**, 031602(R) (2011).
- [27] T. Cap, K. Siwek-Wilczyńska, and J. Wilczyński, *Phys. Rev. C* **83**, 054602 (2011).
- [28] T. Cap, K. Siwek-Wilczyńska, M. Kowal, and J. Wilczyński, *Phys. Rev. C* **88**, 037603 (2013).
- [29] X. J. Bao, S. Q. Guo, H. F. Zhang, and J. Q. Li, *Phys. Rev. C* **96**, 024610 (2017).
- [30] K. Hagino, *Phys. Rev. C* **98**, 014607 (2018).
- [31] X.-J. Lv, Z.-Y. Yue, W.-J. Zhao, and B. Wang, *Phys. Rev. C* **103**, 064616 (2021).
- [32] X.-Q. Deng and S.-G. Zhou, *Phys. Rev. C* **107**, 014616 (2023).
- [33] K. Siwek-Wilczyńska, T. Cap, M. Kowal, A. Sobiczewski, and J. Wilczyński, *Phys. Rev. C* **86**, 014611 (2012).
- [34] T. Cap, M. Kowal, and K. Siwek-Wilczyńska, *Phys. Rev. C* **105**, L051601 (2022).
- [35] C. Simenel, *Eur. Phys. J. A* **48**, 152 (2012).
- [36] T. Nakatsukasa, K. Matsuyanagi, M. Matsuo, and K. Yabana, *Rev. Mod. Phys.* **88**, 045004 (2016).
- [37] C. Simenel and A. Umar, *Prog. Part. Nucl. Phys.* **103**, 19 (2018).
- [38] P. Stevenson and M. Barton, *Prog. Part. Nucl. Phys.* **104**, 142 (2019).
- [39] K. Sekizawa, *Front. Phys.* **7**, 20 (2019).
- [40] X.-X. Sun and L. Guo, *Commun. Theor. Phys.* **74**, 097302 (2022).
- [41] K. Washiyama and D. Lacroix, *Phys. Rev. C* **78**, 024610 (2008).
- [42] A. S. Umar, V. E. Oberacker, J. A. Maruhn, and P.-G. Reinhard, *Phys. Rev. C* **81**, 064607 (2010).
- [43] C. Simenel, M. Dasgupta, D. J. Hinde, and E. Williams, *Phys. Rev. C* **88**, 064604 (2013).
- [44] L. Guo, C. Shen, C. Yu, and Z. Wu, *Phys. Rev. C* **98**, 064609 (2018).
- [45] A. Wakhle, C. Simenel, D. J. Hinde, M. Dasgupta, M. Evers, D. H. Luong, R. du Rietz, and E. Williams, *Phys. Rev. Lett.* **113**, 182502 (2014).
- [46] A. S. Umar, V. E. Oberacker, and C. Simenel, *Phys. Rev. C* **92**, 024621 (2015).
- [47] A. S. Umar, V. E. Oberacker, and C. Simenel, *Phys. Rev. C* **94**, 024605 (2016).
- [48] M. Morjean, D. J. Hinde, C. Simenel, D. Y. Jeung, M. Airiau, K. J. Cook, M. Dasgupta, A. Drouart, D. Jacquet, S. Kalkal, C. S. Palshetkar, E. Prasad, D. Rafferty, E. C. Simpson, L. Tassan-Got, K. Vo-Phuoc, and E. Williams, *Phys. Rev. Lett.* **119**, 222502 (2017).
- [49] K. Godbey, A. S. Umar, and C. Simenel, *Phys. Rev. C* **100**, 024610 (2019).
- [50] K. Godbey and A. S. Umar, *Front. Phys.* **8**, 40 (2020).
- [51] T. Tanaka, D. J. Hinde, M. Dasgupta, E. Williams, K. Vo-Phuoc, C. Simenel, E. C. Simpson, D. Y. Jeung, I. P. Carter, K. J. Cook, N. R. Lobanov, D. H. Luong, C. Palshetkar, D. C.

- Rafferty, and K. Ramachandran, *Phys. Rev. Lett.* **127**, 222501 (2021).
- [52] L. Li, L. Guo, K. Godbey, and A. S. Umar, *Phys. Lett. B* **833**, 137349 (2022).
- [53] A. S. Umar and V. E. Oberacker, *Phys. Rev. C* **74**, 021601(R) (2006).
- [54] N. Wang, X. Wu, Z. Li, M. Liu, and W. Scheid, *Phys. Rev. C* **74**, 044604 (2006).
- [55] C. Simenel, R. Keser, A. S. Umar, and V. E. Oberacker, *Phys. Rev. C* **88**, 024617 (2013).
- [56] C. Simenel, A. S. Umar, K. Godbey, M. Dasgupta, and D. J. Hinde, *Phys. Rev. C* **95**, 031601(R) (2017).
- [57] L. Guo, C. Simenel, L. Shi, and C. Yu, *Phys. Lett. B* **782**, 401 (2018).
- [58] K. Sekizawa and K. Hagino, *Phys. Rev. C* **99**, 051602(R) (2019).
- [59] X.-X. Sun and L. Guo, *Phys. Rev. C* **105**, 054610 (2022).
- [60] K. Banerjee, D. J. Hinde, M. Dasgupta, E. C. Simpson, D. Y. Jeung, C. Simenel, B. M. A. Swinton-Bland, E. Williams, I. P. Carter, K. J. Cook, H. M. David, Ch. E. Düllmann, J. Khuyagaabaatar, B. Kindler, B. Lommel, E. Prasad, C. Sengupta, J. F. Smith, K. Vo-Phuoc, J. Walshe *et al.*, *Phys. Rev. Lett.* **122**, 232503 (2019).
- [61] L. Guo and T. Nakatsukasa, *EPJ Web Conf.* **38**, 09003 (2012).
- [62] L. Guo, K. Godbey, and A. S. Umar, *Phys. Rev. C* **98**, 064607 (2018).
- [63] K. Godbey, L. Guo, and A. S. Umar, *Phys. Rev. C* **100**, 054612 (2019).
- [64] X.-X. Sun, L. Guo, and A. S. Umar, *Phys. Rev. C* **105**, 034601 (2022).
- [65] K. Hagino, N. Rowley, and A. T. Kruppa, *Comput. Phys. Commun.* **123**, 143 (1999).
- [66] D. A. Pigg, A. S. Umar, and V. E. Oberacker, *Comput. Phys. Commun.* **185**, 1410 (2014).
- [67] W. J. Świątecki, K. Siwek-Wilczyńska, and J. Wilczyński, *Acta Phys. Pol. B* **34**, 2049 (2003).
- [68] V. F. Weisskopf and D. H. Ewing, *Phys. Rev.* **57**, 472 (1940).
- [69] N. Bohr and J. A. Wheeler, *Phys. Rev.* **56**, 426 (1939).
- [70] J. D. Jackson, *Can. J. Phys.* **34**, 767 (1956).
- [71] J. Maruhn, P.-G. Reinhard, P. Stevenson, and A. Umar, *Comput. Phys. Commun.* **185**, 2195 (2014).
- [72] X.-X. Sun and L. Guo, *Phys. Rev. C* **107**, L011601 (2023).
- [73] Z. Wu and L. Guo, *Phys. Rev. C* **100**, 014612 (2019).
- [74] Z. Wu and L. Guo, *Sci. China Phys. Mech. Astron.* **63**, 242021 (2020).
- [75] Z. Wu, L. Guo, Z. Liu, and G. Peng, *Phys. Lett. B* **825**, 136886 (2022).
- [76] X. Li, Z. Wu, and L. Guo, *Sci. China Phys. Mech. Astron.* **62**, 122011 (2019).
- [77] E. Chabanat, P. Bonche, P. Haensel, J. Meyer, and R. Schaeffer, *Nucl. Phys. A* **635**, 231 (1998).
- [78] L. Zhu, Z.-Q. Feng, C. Li, and F.-S. Zhang, *Phys. Rev. C* **90**, 014612 (2014).
- [79] K. Nishio, S. Mitsuoka, I. Nishinaka, H. Makii, Y. Wakabayashi, H. Ikezoe, K. Hirose, T. Ohtsuki, Y. Aritomo, and S. Hofmann, *Phys. Rev. C* **86**, 034608 (2012).
- [80] A. S. Umar and V. E. Oberacker, *Nucl. Phys. A* **944**, 238 (2015).
- [81] P. D. Stevenson, *Front. Phys.* **10**, 1019285 (2022).
- [82] P. Jachimowicz, M. Kowal, and J. Skalski, *At. Data Nucl. Data Tables* **138**, 101393 (2021).
- [83] Y. T. Oganessian, V. K. Utyonkov, Y. V. Lobanov, F. S. Abdullin, A. N. Polyakov, I. V. Shirokovsky, Y. S. Tsyganov, G. G. Gulbekian, S. L. Bogomolov, B. N. Gikal, A. N. Mezentsev, S. Iliev, V. G. Subbotin, A. M. Sukhov, A. A. Voinov, G. V. Buklanov, K. Subotic, V. I. Zagrebaev, M. G. Itkis, J. B. Patin *et al.*, *Phys. Rev. C* **70**, 064609 (2004).